Volume 1 | Number 1 | Jan 2013 | Pages 1–100

Nanoscale

www.rsc.org/nanoscale

ROYAL SOCIETY OF CHEMISTRY

ROYAL SOCIETY OF CHEMISTRY

www.rsc.org/nanoscale

Nanoscale

ARTICLE TYPE

Facile synthesis of Au-SnO$_2$ hybrid nanospheres with enhanced photoelectrochemical biosensing performance

Qingming Shen,*[a] Jingyi Jiang,[a] Shilei Liu,[a] Li Han,[a] Xiaohui Fan,[a] Mengxing Fan,[a] Quli Fan,[a] Lianhui Wang,[a] Wei Huang*[ab]

Au-SnO$_2$ hybrid nanospheres (HNSs) were synthesized by a facile, one-step method, which was achieved via a redox reaction between the reductive stannous (II) ions and oxidative auric (III) ions and dissolved O$_2$, and then in situ formation of Au nanoparticles (NPs) and SnO$_2$ NPs. The results indicated that the Au
10 NPs are able to trap electrons, improve the electron-hole pairs' life, and enhance the visible light absorption intensity that are all beneficial for enhancement of the visible light photoelectrochemical performance. The cysteine was chosen as a model molecular to fabricate the photoelectrochemical biosensor. The biosensor displayed excellent analytical performance for detection of cysteine with an extremely broad linear range from 0.4 μM to12 mM), and a low detection limit (0.1 μM). Therefore, the
15 Au-SnO$_2$ HNSs will be a promising candidate for photocatalysts, photoelectrochemical biosensor, and other photoelectric devices.

Introduction

To incorporate new functionalities and improve the physical and chemical properties, various nanoscale oxide-based materials
20 are combined with noble metal nanoparticles (NPs) to form hybrid noble metal-oxide nanostructures, which combining different properties into a single structure. The synergistic properties exceed the functionality of the individual components and bring about new functionalities for a wide range of promising
25 applications, including labelling/sensing,[1,2] solar energy conversion,[3] catalysis,[4] lithium ion electrode materials,[5] field emission emitters[6] and electronic devices[7] et al. To date, a number of M-oxides nanostructures have been designed and prepared, such as M-SiO$_2$[8] M-SnO$_2$,[9] M-TiO$_2$,[10] M-CeO$_2$,[11] and
30 M-ZnO[12] (M= Ag, Au, Pd, Pt).

As one of the most extensively studied hybrid nanostructures, Au-SnO$_2$ system has attracted great attention because of their highly enhanced optical, electronic and catalytic performance. First of all, SnO$_2$ is one of the post-transition metal oxide and n-
35 type wide-bandgap (E_g =3.6 eV) semiconductor[13-15] with high thermal and chemical stability,[16] low toxicity, low cost, and high electron mobility.[17] Specifically, the electron mobility of SnO$_2$ is ~250 cm^{2}V^{-1}s^{-1},[18] which is remarkably larger than the <1 cm^{2}V^{-1}s^{-1} of conventional TiO$_2$ photoanode materials.[19] Besides, SnO$_2$ has
40 low electrical resistance and high optical transparency in the visible range which make it a promising anode material for optoelectronic devices.[20] Furthermore, the doped Au NPs could significantly enhanced the photoelectric properties of SnO$_2$, which was likely attributed to the following reasons: (1) When
45 Au NPs is doped into the SnO$_2$, a Schottky barrier could be formed in the interfacial region of Au and SnO$_2$.[21, 22] The

presence of Schottky barrier is favourable for the separation of electrons and holes and prevented the recombination of electron–hole pairs. The internal electric field existing in hetero-junctions
50 between SnO$_2$ and Au NPs could induce faster carrier migration, thus enhancing the photoelectrochemical performance. (2) The doped Au NPs could increase the visible light absorption due to the strong surface plasmon resonance (SPR) of Au NPs.[23] (3) The presence of Au NPs could improve the conductivity of the
55 electrode due to the good carrier transport property of Au NPs. By far, several methods have been reported to synthesize Au-SnO$_2$ nanocomposites such as microwave hydrothermal method,[24] deposition-precipitation,[25] intermetallics-based dry oxidation method.[26] However, the synthesis procedures
60 mentioned above either needed harsh reaction conditions or complex operations, and the irregular morphology and agglomerate of the samples limited their applications. Therefore, it is urgent to develop a simple method for the fabrication of Au-SnO$_2$ hybrids with well-designed and controlled nanostructures.
65 In the present work, uniform Au-SnO$_2$ hybrid nanospheres (HNSs) were synthesized via a facile, one-step method. The synthesis procedure of Au-SnO$_2$ HNSs was achieved via a redox reaction between the reductive stannous (II) ions and oxidative auric (III) ions and dissolved O$_2$, and then in situ formation of Au
70 NPs and SnO$_2$ NPs. The results indicated that the as-prepared Au-SnO$_2$ HNSs were composed by tens of SnO$_2$ NPs (~3 nm) and Au NPs (5~7 nm). The surrounded SnO$_2$ NPs acted as physical barriers to protect the Au NPs from aggregation. The Au NPs were embedding into the SnO$_2$ HNSs, with a nanostructure
75 similar to the plum-pudding model proposed by Thomson.[27] The photoelectrochemical biosensing performance of the Au-SnO$_2$ HNSs was explored through monitoring their photocurrent

response to cysteine. The result indicated that the photoelectrochemical biosensor showed a considerable wide linear range to cysteine, from 0.4 µM to 12 mM. The detection limit of this biosensor was about 0.1 µM at a signal-to-noise ratio of 3. Thus it could be seen that the Au-SnO$_2$ HNSs presented promising applications in the fields of photoelectrochemical biosensor and photoelectric devices.

Experimental Section

Chemicals

SnCl$_2$·2H$_2$O, NaOH, NaH$_2$PO$_4$, Na$_2$HPO$_4$, Cd(NO$_3$)$_2$·6H$_2$O, Na$_2$S·9H$_2$O and polyvinylpyrrolidone (PVP) were purchased from Sinopharm Chemical Reagent Co. Ltd., HAuCl$_4$·4H$_2$O was purchased from Shanghai Chemical Reagent Co. Ltd. Ethanol was purchased from Aladdin Reagent Co. Ltd. All reagents were of analytical purity and were used without further purification. All aqueous solutions were prepared with ultrapure water (18 MΩ·cm^{-1}), which was obtained from a Milli-Q water purification system.

Synthesis of Au-SnO$_2$ HNSs

PVP (0.3 g) and SnCl$_2$·2H$_2$O (0.5 mmol) were dissolved into 40 mL absolute ethanol under stirring at room temperature under the N$_2$ protection. Then 0.5 mL aqueous solution of HAuCl$_4$ (24.3 mM) was added into the above solution. After 2 min, 3.5 mL NaOH aqueous solution (1.0 M) was slowly added to above mixture solution, then followed by added 16.5 mL of H$_2$O. The solution was maintained at 60 °C with stirring for 3 h. The final purple-red precipitate was collected by centrifugation, and washed with ethanol and water for several times, then dried at 60 °C for 12 h.

Synthesis of SnO$_2$ NSs

Pristine SnO$_2$ NSs were prepared using the same method without adding HAuCl$_4$ solution.

Fabrication of Au-SnO$_2$/CdS modified ITO electrodes (ITO/Au-SnO$_2$/CdS)

Indium tin oxide (ITO) slices (sheet resistance 20 Ω/square) were sonicated in isopropanol, ethanol, and water for 15 min, respectively. Then, 20 µL of the Au-SnO$_2$ HNSs dispersion solution (5.0 mg mL^{-1}) was drop-cast onto a piece of ITO slice with an area of 0.25 cm^2. After drying in air, the film was calcined at 400 °C for 30 min to remove any organic compounds and improve the contact between the HNSs and the substrate. Pristine SnO$_2$ films were also made using the same method. The Au-SnO$_2$ HNSs coated ITO is referred as an ITO/Au-SnO$_2$ electrode. The CdS NPs were deposite on the Au-SnO$_2$ HNSs surface through a successive ionic layer adsorption and reaction technique.[28] In brief, the ITO/Au-SnO$_2$ electrode was immersed alternately in Cd^{2+} and S^{2-} solution in an aqueous solution of 0.08 M [Cd(NH$_3$)$_4$]$^{2+}$ and 0.1 M Na$_2$S at room temperature for 30 s, respectively. The ITO/Au-SnO$_2$/CdS electrode with 6 layers was fabricated, and then rinsed thoroughly with water and air dried.

Characterization

The morphology of the samples was characterized by scanning electron microscopy (SEM, Hitachi S4800) and transmission electron microscopy (TEM, Hitachi HT7700). High-resolution transmission electron microscopy (HRTEM) was performed using a JEOL-2100 high resolution transmission electron microscope with an accelerating voltage of 200 kV. Energy dispersive X-ray (EDX) analysis was obtained with an Oxford INCA detector installed on the HRTEM. Ultraviolet-visible (UV–Vis) absorption spectrum was measured using a Shimadzu UV-3600 UV/vis spectrophotometer. X-ray diffractometer (XRD) analysis was carried out using Rigaku XRD with Cu Kα (λ=0.15418 nm) source with a Ni filter. Electrochemical impedance spectroscopy (EIS) was carried out on an Autolab potentiostat/galvanostat (PGSTAT30, Utrecht, The Netherlands) in 0.1 M KCl containing a redox probe of 10.0 mM K$_3$[Fe(CN)$_6$]/K$_4$[Fe(CN)$_6$] (1:1) mixture at an open-circuit potential of 216 mV with an applied voltage of 5 mV over a frequency range of 0.1 Hz-100 kHz. Dynamic light scattering (DLS) measurements was performed using a Brookhaven instrument (90 Plus/BI-MAS) equipped with a 15 mW solid state laser with an output at a scattering angle of 90°.

Photoelectrochemical Measurements and L-Cysteine Sensing

photoelectrochemical measurements were performed with a homemade photoelectrochemical system. A 500 W Xe lamp equipped with a monochromator was used as the irradiation source. Photocurrent was measured on a CHI 660D electrochemical workstation. ITO/Au-SnO$_2$/CdS, ITO/ SnO$_2$/CdS, ITO/Au-SnO$_2$, ITO/SnO$_2$ electrodes were employed as the working electrode. A Pt wire electrode and Ag/AgCl electrode were used as the counter electrode and reference electrode, respectively. Phosphate buffer solution (PBS, pH 7.4, 0.1 M) containing 10 mM Cysteine was used as the electrolyte for photocurrent measurements. The solution was deaerated with nitrogen for 15 min before experiments, and then a N$_2$ atmosphere was kept in the entire experimental process.

Results and discussion

Reaction mechanism of Au-SnO$_2$ HNSs

According to the standard electrode potential, Sn^{2+} (Sn^{4+} + 2e→Sn^{2+}, E$^\theta$ = +0.154 V), which is much lower than that of AuCl$_4^-$ (AuCl$_4^-$ +3e$^-$→Au^0, E$^\theta$ = +1.50V). As a result, the auric (III) ions were reduced by stannous (II) ions and the stannous (II) ions were oxidized by auric (III) ions and dissolved O$_2$.[29, 30] After adding NaOH solution, the stannic (IV) ions were then in situ hydrolyzed to Sn(OH)$_6^{2-}$, and easily dehydrating to SnO$_2$, and the formed Au NPs were surrounded by the SnO$_2$ NPs. The possible reaction equation of Au-SnO$_2$ HNSs can be considered as follows:

$$Sn^{2+} + AuCl^{4-} \rightarrow Sn^{4+} + Au^0 \qquad (1)$$
$$Sn^{2+} + O_2 + H_2O \rightarrow Sn^{4+} + OH^- \qquad (2)$$
$$Sn^{4+} + OH^- \rightarrow Sn(OH)_6^{2-} \qquad (3)$$
$$Sn(OH)_6^{2-} \rightarrow SnO_2 + H_2O \qquad (4)$$

From (1), (2), (3), we can obtained the equation:

$$3Sn^{2+} + 2AuCl^{4-} + 12OH^- \rightarrow 3SnO_2 + 2Au + 6H_2O \quad (5)$$
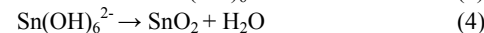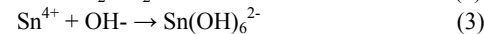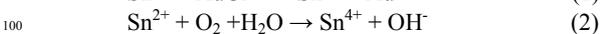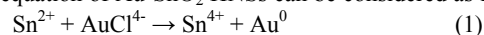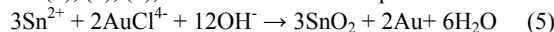
Characterization of Au-SnO$_2$ HNSs

The morphology of the as-prepared Au-SnO$_2$ HNSs was investigated by SEM and TEM. From the images (Fig. 1A & 1C) of the panoramic morphology, the as-obtained sample showed a uniform spheres structure with the average diameter of 150 nm. The particle sizing distribution also confirmed that the major diameter was 160 nm (inset in Fig. 1A). The Au NPs were highly dispersed in the SnO$_2$ HNSs. This was believed to favour the photogenerated electron transfer between the gold and SnO$_2$.[31] Moreover, the enlarged SEM and TEM images shown in Fig. 1B & D revealed that the Au NPs with the diameter of 5~8 nm

decorated in the SnO$_2$ NSs, which was quite similar to the structure of the plum-pudding model proposed by Thomson.[27] The HRTEM image indicated that the SnO$_2$ nanospheres were polycrystalline. The clear preferential lattice orientation in Fig. 1E confirmed that the Au-SnO$_2$ HNSs were composed of several small nanograins. The clearly marked interplanar spacing d$_1$ was 0.336 nm, which corresponded to the (110) lattice planes of cassiterite SnO$_2$. The interplane distance d$_2$ of 0.23 nm could be attributed to the (111) plane of Au. Furthermore, detailed analysis of the HRTEM results confirmed that the Au-SnO$_2$ hybrid HNSs were assembled by tens of SnO$_2$ primary NPs with a dimension of ~3 nm and Au nanoparticles with a dimension of ~5 nm. In the HNSs, SnO$_2$ played the key role of physically separating the Au NPs from each other. The steric hindrance of the SnO$_2$ NPs benefit to keeping the original shape, size, surface state, and activity of Au NPs. In addition, the doped Au NPs greatly enhanced the photoelectrochemical response ability of SnO$_2$, because the Au NPs acted as a reservoir of photoelectrons, improving the interfacial charge-transfer and retarding the recombination of photoexcited electron-holes.[32] The energy dispersive spectrum in Fig. 1F confirmed the presence of Au element and the content percent was about 2.0 %. The element ratio of Sn to O was 1: 2, which also confirmed the composite of Au-SnO$_2$.
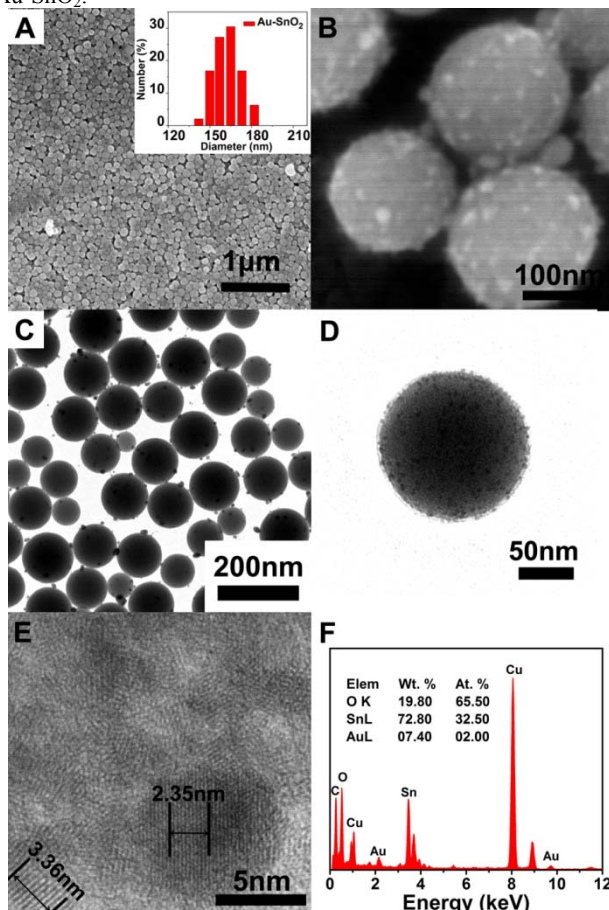
Fig. 1 A, B) SEM images of as-prepared Au-SnO$_2$ HNSs and DLS of particle diameters (inset of image A). C, D) TEM images of Au-SnO$_2$ HNSs. E) HRTEM images of Au-SnO$_2$ HNSs. F) The EDS spectra of Au-SnO$_2$ HNSs.

The crystal structure of the Au-SnO$_2$ HNS was further characterized by X-ray diffractometer (XRD). As shown in pattern a (Fig. 2), all the peaks could be assigned to the tetragonal rutile structure of SnO$_2$ with the lattice parameters of a= 0.4736

and c= 0.3186, which agrees with the standard data (JCPDS # 41-1445). In pattern b, for Au-SnO$_2$ HNSs, except for the four strong SnO$_2$ peaks (110), (101), (211) and (112), the presence of Au (111), (200) and (311) peaks could be well assigned to face-centered cubic Au (JCPDS # 65-2870).
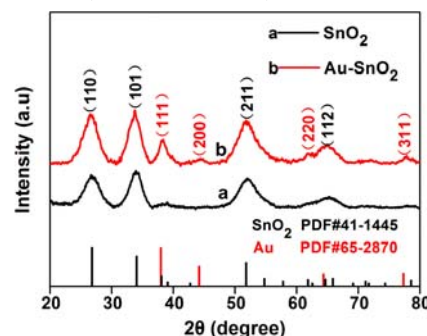
Fig. 2 XRD patterns of Au-SnO$_2$ HNSs and SnO$_2$ NSs.
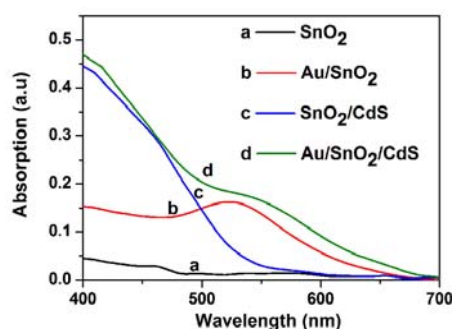
Fig. 3 UV-vis absorption spectra of the different nanostructures modified-ITO electrodes: (a) SnO$_2$ NSs, (b) Au-SnO$_2$ HNSs, (c) SnO$_2$/CdS and (d) Au-SnO$_2$/CdS.
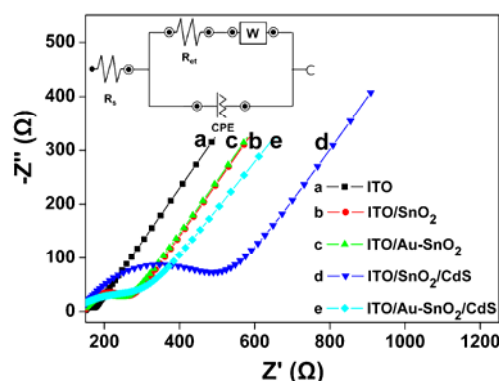
Fig. 4 Electrochemical impedance Nyquist plot and quivalent circuit (inset) of modified ITO electrodes: (a) ITO, (b) ITO/SnO$_2$, (c) ITO/Au-SnO$_2$, (d) ITO/SnO$_2$/CdS and (e) ITO/ Au-SnO$_2$/CdS.

Fig. 3 shows the UV-vis absorption spectra of SnO$_2$, Au-SnO$_2$, SnO$_2$/CdS and Au-SnO$_2$/CdS. Compared with the absorption spectra of SnO$_2$ and SnO$_2$/CdS films (curve a & c, Fig. 3), Au-SnO$_2$ and Au-SnO$_2$/CdS films (curve b & d, Fig. 3) offered the obvious absorption peaks around 540 nm, which matched very well with the characteristic SPR spectra of Au NPs. Meanwhile, as a sensitizer, the decorated CdS NPs significantly enhanced the whole absorption in visible light. It was concluded that both Au NPs and CdS NPs enhanced the visible absorption intensity of SnO$_2$ films.

The introduction of Au NPs could improve the conductivity of the electrode due to the good carrier transport property of Au NPs.

To gain further insight into the electron-transport properties of the Au-SnO$_2$ HNSs, electrochemical impedance spectroscopy (EIS) of different electrodes was measured using K$_3$Fe(CN)$_6$/K$_4$Fe(CN)$_6$ as a redox probe (Fig. 4). The diameter of the semicircle was equal to the electron-transfer resistance (R$_{et}$). It can be seen that after the SnO$_2$ and CdS were coated onto ITO, R$_{et}$ increased (curve b & d, Fig. 4), indicating that the formed compact SnO$_2$ or CdS NPs hindered the access of the redox probe ([Fe(CN)$_6$]$^{3-}$/[Fe(CN)$_6$]$^{4-}$) to the electrode surface. However, in the case of ITO/Au-SnO$_2$ and ITO/ Au-SnO$_2$/CdS (curve c & e, Fig. 4), the embedding of Au NPs promoted the transfer of the redox probe to the electrode, and thus led to a decrease of the R$_{et}$ value, which smaller than that of the electrode without Au NPs (curve b, d, Fig. 4)

Photoelectrochemical measurements

The photoelectrochemical performance of the Au-SnO$_2$ HNSs was studied using CdS QDs as photosensitizer. The structure of the Au-SnO$_2$ HNSs photoanode was shown in Fig. 5A, the Au NPs were embedding in the SnO$_2$ NS, which could not only arouse the SPR effect, but also enhance the conductivity of SnO$_2$ NS. In addition, the introduction of narrow band gap CdS QDs as photosensitizer was favourable for the generation and separation of electron-hole pairs under visible-light.[33] As shown in Fig. 5B, upon irradiation with visible light (> 420 nm), the ITO/SnO$_2$ electrode showed a photocurrent of 27 nA at an applied potential of 0 V (curve a), whereas the ITO/Au-SnO$_2$ electrode showed a photocurrent of 84 nA (curve b), indicating the obvious enhancement of the photo-current conversion efficiency of SnO$_2$ by the addition of Au NPs. After sensitized by CdS NPs, the photocurrent of the ITO/SnO$_2$ electrode and ITO/Au-SnO$_2$ were both significant enhanced, they reached to 13.6 μA and 44.3 μA, respectively (curve c, d). It should be noted that the photocurrent for an electrode containing Au NPs was about three times higher than that for the electrode without Au NPs. In this case, the incorporation of the Au NPs mainly acted as a sink for photo-induced electrons and decreases the recombination of photo-generated electrons to enhance the photocurrent of the composite film. The enhanced photocurrent of Au-SnO$_2$ HNSs makes them to be a promising candidate for the fabrication of photoelectrochemical biosensor.

Photoelectrochemical sensing of cysteine

Cysteine, as an essential sulphur-containing amino acid, plays a critical role in many biological processes. Diseases like slow growth, leucocyte loss, and liver, edema, muscle, and skin lesions were observed to be accompanied by a deficiency of cysteine.[34-36] According to the literature, photoelectrochemical method was a rapid and sensitive technique for testing cysteine.[37-39] Therefore, the as-prepared Au-SnO$_2$ HNSs were used to fabricate cysteine biosenser by photoelectrochemical method. The mechanism for the measurement of cysteine was displayed in Fig. 6A. Cysteine, as eletron donor, scavenged the hole of the excited CdS under visible-light irradiation. The photoexcitation electrons of CdS could transfer from its valence band (VB, -6.38 eV) to its conduction band (CB, -3.98 eV), then injected to the CB of SnO$_2$ (-4.50 eV). Au NPs, which served as an electron relay, to induce the electron transfer from SnO$_2$ to the ITO electrode, thus resulting in an efficient charge transport and an enhanced photocurrent signal. In this process, cysteine serviced as the electron donor (hole scavenger) and sacrificial reagent can transfer electrons to the holes located on the excited state of CdS, avoiding electron-hole recombination effectively, leading to a sharp increase of the photocurrent. Au NPs acted as not only electron traps for facilitating charge separation, but also the light trapping or scattering agent.[40-42] Due to the superior electrical conductivity of Au, it serves as an excellent electron-transport matrix to capture electrons and transport electrons from excited CdS to ITO rapidly, avoiding electron-hole recombination effectively, resulting in a much more sensitive response to visible light. To verify the performance of the photoelectrochemical sensor in the determination of cysteine, its photocurrent response with increasing concentration of cysteine was measured (Fig. 6B). The photocurrent response showed a linear relationship with the logarithm of cysteine concentration under visible light illumination (> 420 nm). The linear response range was from 0.4 μM to 12 mM (Fig. 6C), which was wider than the previous reports, as shown in Table. 1. The detection limit was estimated to be 0.1 μM at a signal-to-noise ratio of 3. Since the normal level of cysteine in human plasma is in the range of 240-360 μM,[43, 44] the present biosensor showed enough sensitivity for the detection of cysteine in real samples.
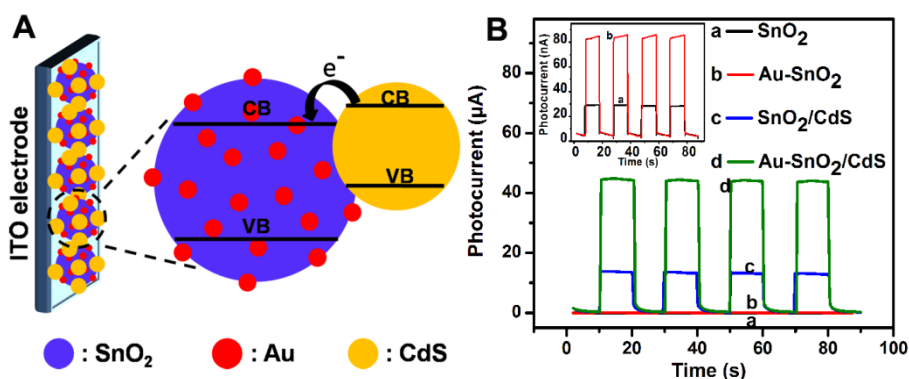
Fig. 5 A) Schematic illustration of an ITO/Au-SnO$_2$/CdS film. B) Photocurrent responses of (a) SnO$_2$, (b) Au-SnO$_2$ (c) SnO$_2$/CdS and (d) Au-SnO$_2$/CdS modified ITO electrodes in 0.1 M PBS (pH 7.4) containing 10 mM cysteine. The applied potential was 0 V, the light wavelength was > 420 nm.
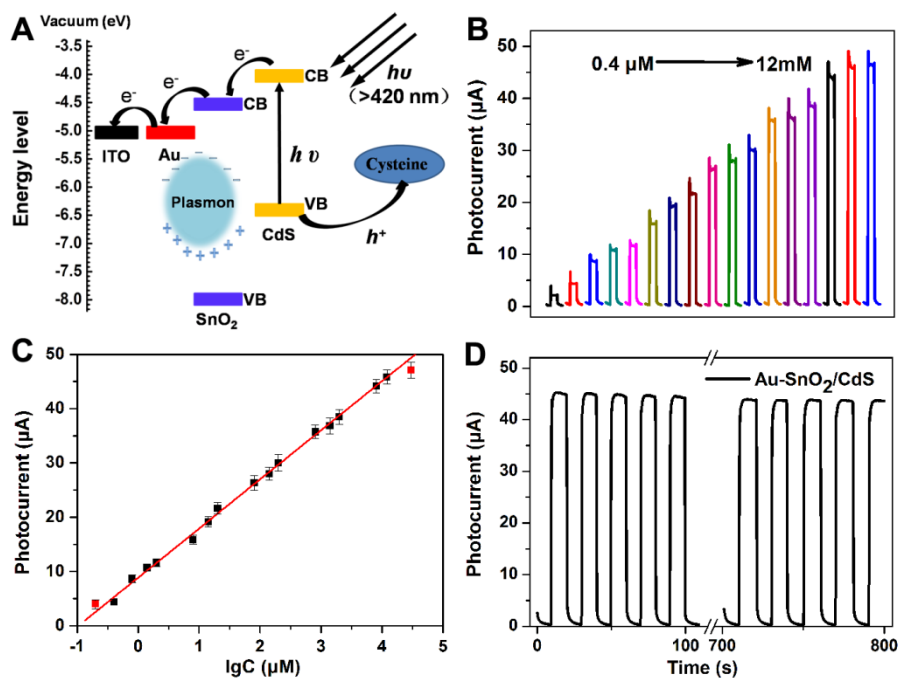
Fig. 6 A) The schematic illustration of electron-transfer process at the Au-SnO$_2$/CdS/ITO electrode under visable light. B) Photocurrent responses of ITO/Au-SnO$_2$/CdS in 0.1 M PBS (pH 7.4) in the presence of the cysteine ranging from 0.4 µM to 12 mM (from left to right) at 0 V under illumination with the visible light (> 420 nm). C) linear calibration curve according to Fig. B. D)Time-based photocurrent response of the ITO/Au-SnO$_2$/CdS electrode in 0.1 M pH 7.4 PBS containing 10 mM cysteine with irradiation on/off repeated every 10 s.

Table. 1 Comparison of the cysteine detection by different methods

Method	Linear range	Detection limit	Reference
UV absorption spectra	5 – 250 µM	0.04 µM	[43]
Electrochemical	18 – 1000 µM	50 nM	[44]
Fluorescence spectra	2.5 – 110 nM	5.1 nM	[45]
Photoelectrochemical	0.2 – 2.8 µM	0.1 µM	[37]
Photoelectrochemical	0.6 – 157 µM	0.2 µM	[38]
Photoelectrochemical	0.1 – 100 µM	25 nM	[39]
Photoelectrochemical	0.4 – 12, 000 µM	0.1 µM	This work

In addition, the stability of the photoelectrochemical biosensor was examined in the presence of 10 mM cysteine. From Fig. 6D, we could find that after 800 s, the photocurrent intensity still remained 97.7 % of the initial value, suggesting a good stability of the Au-SnO$_2$/CdS-modified film. The repeatability of the photoelectrochemical biosensor was tested at the cysteine concentrations of 100 µM. The relative standard deviation for five measurements was 4.7 %, thus giving a good repeatability. Moreover, the response could reach the steady signal within 5 s, which made the strategy more convenient with a shorter detection time.

In order to evaluate the selectivity of the photoelectrochemical sensor, we measured its photoresponse toward cysteine and other ten different types of amino acids. Arginine, asparagine, glutamine, alanine, histidine, lysine, phenylalanine, proline, serine and methionine at ten folds concentration of cysteine had no obvious influence on the photoelectrochemical response of cysteine (Fig. 7). Therefore, the as-prepared photoelectrochemical biosensor would have good discrimination ability for monitoring of cysteine in amino acid samples.
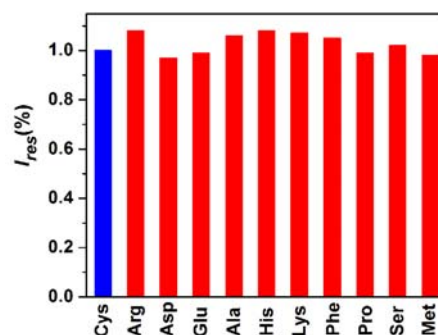
Fig. 7 Photocurrent response of Au-SnO$_2$/CdS/ITO electrodes upon addition of 10 mM of arginine (Arg), asparagines (Asp), glutamine (Glu), alanine (Ala), histidine (His), lysine (Lys), phenylalanine (Phe), proline (Pro), serine (Ser) and methionine (Met) to 0.1 M PBS (pH 7.4) containing 1 mM cysteine, respectively. The applied potential was 0 V, the light wavelength was > 420 nm.

Conclusion

In summary, Au-SnO$_2$ HNSs were successfully prepared through a facile, clean and one-step method. These uniform Au-SnO$_2$ HNSs are completely built up by spontaneous self-assembly of Au and SnO$_2$ NPs. The Au-SnO$_2$ HNSs combined with CdS NPs could be used to fabricate photoelectrochemical cysteine biosensor. It appeared a broad linear range from 0.4 µM to 12 mM with a detection limit of 0.1 µM. This proposed biosensor shows good performance and high applied potential in the field of biological detection for its advantages such as rapid response, wide concentration range, low cost, and good reproducibility. This simple approach can be a useful method for making

nanostructures of other metals-SnO_2 HNSs with different component, which can be used in the fields of catalysis, photoelectrochemical devices and biosensors.

Acknowledgements

Notes and references

[a] *Key Lab of Organic Electronics & Information Displays, Institute of Advanced Materials, Nanjing University of Posts and Telecommunications, Nanjing, 210023, People's Republic of China. Email: iamqmshen@njupt.edu.cn, iamwhuang@njtech.edu.cn.; Tel.: +86 25 85866533; fax: +86 25 85866396.*

[b] *Jiangsu-Singapore Joint Research Center for Organic/Bio-Electronics & Information Displays and Institute of Advanced Materials, Nanjing Tech University, Nanjing 211816, People's Republic of China*

1. C. Xue, X. Chen, S. J. Hurst, C. A. Mirkin, *Adv. Mater.* 2007, **19**, 4071-4074.
2. S. Liu, Y. Wong, Y. Wang, D.Wang, M. Y. Han, *Adv. Funct. Mater.* 2007, **17**, 3147-3152.
3. P. V. Kamat, *J. Phys. Chem. C* 2008, **112**, 18737-18753.
4. H. P. Zhou, H. S. Wu, J. Shen, A. X. Yin, L. D. Sun, C. H. Yan, *J. Am. Chem. Soc.* 2010, **132**, 4998-4999.
5. S. Gao, S. Yang, J. Shu, S. Zhang, Z. Li, K. Jiang, *J. Phys. Chem. C* 2008, **112**, 19324-19328.
6. Y. Zhu, T. Yu, F. Cheong, X. Xu, C. Lim, V. Tan, J. Thong, C. H. Sow, *Nanotechnology* 2005, **16**, 88.
7. M. T. Sheldon, P. E. Trudeau, T. Mokari, L. W. Wang, A. P. Alivisatos, *Nano lett.* 2009, **9**, 3676-3682.
8. Y. Zhai, Y. Dou, D. Zhao, P. F. Fulvio, R. T. Mayes, S. Dai, *Adv. Mater.* 2011, **23**, 4828-4850.
9. C. Zhu, P. Wang, L. Wang, L. Han, S. Dong, *Nanoscale* 2011, **3**, 4376-4382.
10. Z. D. Gao, H. F. Liu, C. Y. Li, Y. Y. Song, *Chem. Commu.* 2013, **49**, 774-776.
11. J. Qi, J. Chen, G. Li, S. Li, Y. Gao, Z. Tang, *Energy. Environ. Sci.* 2012, **5**, 8937-8941.
12. P. Li, Z. Wei, T. Wu, Q. Peng, Y. Li, *J. Am. Chem. Soc.* 2011, **133**, 5660-5663.
13. X. W. Lou, Y. Wang, C. Yuan, J. Y. Lee, L. A. Archer, *Adv. Mater.* 2006, **18**, 2325-2329.
14. X. W. Lou, C. Yuan, L. A. Archer, *Small* 2007, **3**, 261-265.
15. X. W. Lou, J. S. Chen, P. Chen, L. A. Archer, *Chem. Mater.* 2009, **21**, 2868-2874.
16. L. Wang, T. Fei, J. Deng, Z. Lou, R. Wang, T. Zhang, *J. Mater. Chem.* 2012, **22**, 18111-18114.
17. T. Yanagimoto, Y. T. Yu, K. Kaneko, *Sensor Actuat. B-Chem.* 2012, **166**, 31-35.
18. Z. Jarzebski, J. Marton, *J. electrochem. Soc.* 1976, **123**, 299-310.
19. E. Hendry, M. Koeberg, B. O'Regan, M. Bonn, *Nano lett.* 2006, **6**, 755-759.
20. M. Batzill, U. Diebold, *Prog. Surf. Sci.* 2005, **79**, 47-154.
21. E. W. McFarland, J. Tang, *Nature* 2003, **421**, 616-618.
22. J. Du, J. Qi, D. Wang, Z. Tang, *Energy. Environ. Sci.* 2012, **5**, 6914-6918.
23. Z. Zheng, B. Huang, X. Qin, X. Zhang, Y. Dai, M. H. Whangbo, *J. Mater. Chem.* 2011, **21**, 9079-9087.
24. Y. T. Yu, P. Dutta, *J. Solid State Chem.* 2011, **184**, 312-316.
25. S. Wang, J. Huang, Y. Zhao, S. Wang, X. Wang, T. Zhang, S. Wu, S. Zhang, W. Huang, *J. Mol. Catal. A-Chem.* 2006, **259**, 245-252.
26. K. Yu, Z. Wu, Q. Zhao, B. Li, Y. Xie, *J. Phys. Chem. C* 2008, **112**, 2244-2247.
27. K. Hentschel, *Compend. Quant. Phys.*, 2009, **11**.18-21.
28. C. H. Chang, Y. L. Lee, *Appl. Phys. Lett.* 2007, **91**, 053503.
29. H. B. Wu, J. S. Chen, X. W. Lou, H. H. Hng, *J. Phys. Chem. C* 2011, **115**, 24605-24610.
30. J. SongáChen, M. FengáNg, H. BináWu, *CrystEngComm* 2012, **14**, 5133-5136.
31. P. Claus, H. Hofmeister, *J. Phys. Chem. B* 1999, **103**, 2766-2775.
32. G. Oldfield, T. Ung, P. Mulvaney, *Adv. Mater.* 2000, **12**, 1519-1522.
33. Q. Shen, X. Zhao, S. Zhou, W. Hou, J. J. Zhu, *J. Phys. Chem. C* 2011, **115**, 17958-17964.
34. Z. A. Wood, E. Schröder, J. Robin Harris, L. B. Poole, *Trend. biochem. sci.* 2003, **28**, 32-40.
35. S. Shahrokhian, *Anal. chem.* 2001, **73**, 5972-5978.
36. V. Gazit, R. Ben-Abraham, R. Coleman, A. Weizman, Y. Katz, *Amino Acids* 2004, **26**, 163-168.
37. Y. T. Long, C. Kong, D. W. Li, Y. Li, S. Chowdhury, H. Tian, *Small* 2011, **7**, 1624-1628.
38. W. Tu, J. Lei, P. Wang, H. Ju, *Chem-Eur. J.* 2011, **17**, 9440-9447.
39. B. Sun, K. Zhang, L. Chen, L. Guo, S. Ai, *Biosens. Bioelectron.* 2013, **44**, 48-51.
40. D. Schaadt, B. Feng, E. Yu, *Appl. Phys. Lett.* 2005, **86**, 063106.
41. W. Smith, S. Mao, G. Lu, A. Catlett, J. Chen, Y. Zhao, *Chem. Phys. Lett.* 2010, **485**, 171-175.
42. S. Mokkapati, F. Beck, A. Polman, K. Catchpole, *Appl. Phys. Lett.* 2009, **95**, 053115.
43. N. Shao, J. Y. Jin, S. M. Cheung, R. H. Yang, W. H. Chan, T. Mo, *Angew. Chem.* 2006, **118**, 5066-5070.
44. M. Zhou, J. Ding, L. P. Guo, Q. K. Shang, *Anal. chem.* 2007, **79**, 5328-5335.
45. F. Pu, Z. Huang, J. Ren, X. Qu, *Anal. chem.* 2010, **82**, 8211-8216.